Journal of Volcanology and Geothermal Research 452 (2024) 108138

Contents lists available at ScienceDirect

Journal of Volcanology and Geothermal Research

journal homepage: www.journals.elsevier.com/journal-of-volcanology-and-geothermal-research

Optimal spatial distribution of seismic stations to detect magma migration using the seismic amplitude ratio analysis

T. Espinosa-Ortega [a,*], B. Taisne [a,b]

[a] Earth Observatory of Singapore, Nanyang Technological University, Singapore
[b] Asian School of the Environment, Nanyang Technological University, Singapore

ARTICLE INFO

Keywords:
Volcano seismology
Seismic network optimization
Magma migration detection
Features importance

ABSTRACT

Magma migrations frequently trigger seismic swarms, resulting in seismic events that overlap in time and hinder real-time phase picking commonly used for hypocenter location. Addressing this challenge, seismic amplitude ratio analysis (SARA) allows identification of seismic migrations in real-time by simply tracking the relative seismic amplitude between a pair of seismic stations.

This paper aims to identify key statistical features of the seismic network array locations that improve their ability to detect seismic migrations using SARA. We evaluated the capability to detect the most frequently oriented magma migrations in over 100 volcanoes, using a criterion previously proposed to study vertical magma migrations in Piton de la Fournaise. Additionally, we investigate the influence of vent-station proximity on magma conduit coverage and identify the distance ratio that yields improved detection.

Furthermore, we estimate the seismic network efficiency by calculating the detection capability volume per station. We then use the random forest regression algorithm to identify which statistical features of the seismic network location contribute more to the efficiency disparity among different volcanoes. Notably, our findings reveal that optimizing seismic network coverage entails maximizing the standard deviation of relative pair station distances, while maintaining a prescribed minimum separation distance between station pairs. Our results reveal important criteria that can be used to optimize seismic network location design.

1. Introduction

Volcano monitoring needs include multiparametric analysis of seismic, geodetic, geochemical, optical, and thermal data (Ewert et al., 2005; Miller and Jolly, 2014). The complexity of the monitoring network design arises not only from these competing interests but also from the interplay of technical, political, and social factors unique to each volcano. These factors include budget constraints, land accessibility, ground stability, noise levels, and hazard assessments. The balance among these diverse interests often defines the boundaries for considering other specific goals, such as seismic-related targets.

To find the ideal seismic network location, requires to first identify the primary objectives as the strategy can change accordingly (Hardt and Scherbaum, 1994). These objectives often include event localization (Kijko, 1977; Tramelli et al., 2013; Toledo et al., 2020), moment tensor inversion (Lanza and Waite, 2018) and seismic imaging (Curtis, 1999; Maurer et al., 2017), among others. In the context of volcano monitoring, the optimal location for seismic networks should enable the rapid identification of imminent eruptions, considering several key factors.

As magma migrates, the intrusion in the crust causes brittle fracture and fluid/gas resonances that induce seismicity (Lahr et al., 1994; Chouet, 1996; Rubin and Gillard, 1998). Prior to an eruption, seismic swarms frequently occur, during which seismic events overlap, resulting in continuous tremors or events with emergent onsets (McNutt, 1994). These characteristics can hinder phase picking, which can be utilised to determine hypocentre's locations. To overcome this challenge, frequently the hypocentres are estimated using seismic amplitude decay analysis (Battaglia and Aki, 2003), valid for high-frequency, isotropic S-waves (Morioka et al., 2017). However, using the amplitude decay for event location requires the computation of the amplitude of the source wave (Kumagai et al., 2010, 2013, 2019; Eibl et al., 2014; Kurokawa et al., 2016; Ogiso and Yomogida, 2021) and/or instrument and site amplification factors (Taisne et al., 2011; Walsh et al., 2017; Eibl et al., 2017; Caudron et al., 2015, 2018). Moreover, in most cases these methods, involve solving an inversion problem via a grid search, which requires additional post-processing time.

* Corresponding author.
E-mail address: teortega@ntu.edu.sg (T. Espinosa-Ortega).

https://doi.org/10.1016/j.jvolgeores.2024.108138
Received 3 April 2024; Received in revised form 1 July 2024; Accepted 5 July 2024
Available online 6 July 2024

In crisis response situations, an alternative to calculating hypocentres is to use the seismic amplitude ratio analysis (SARA) (Taisne et al., 2011), that by simply computing the evolution of the seismic amplitude ratio between a pair of seismic stations, allows to track seismic migrations, which can be associated to magma migrations (Tan et al., 2019). In a prior study, James et al., 2023 proposed a method for evaluating the detection capability of SARA. The method consisted in calculating the volume under the volcano, where the change of the seismic amplitude ratio along a migration path, was larger than the variability observed in seismic signals. As an example, the potential to detect vertical magma migrations in Piton de la Fournaise was studied.

In this paper, our primary objective is to identify the general characteristics of seismic networks locations that enhance their capacity to detect magma migrations using SARA. To achieve this, we apply James et al., 2023 method to calculate the detection capability of >100 volcanoes, with different topographies, including stratovolcanoes, calderas, shields, complex volcanos, pyroclastic cones, fissure vents, lava domes and somma volcanoes. The seismic network locations around the volcanoes are obtained from the Global Volcano Monitoring Infrastructure Database (GVMID) (Widiwijayanti et al., 2024) hosted by the World Organization of Volcano Observatories database, WOVOdat (Newhall et al., 2017; Costa et al., 2019); and the EarthScope Consortium web service *(https://service.iris.edu/)*. The topography of the volcanoes is obtained using the Shuttle Radar Topography Mission (STRM) open data (Rabus et al., 2003; Farr et al., 2007). The volcanic vents are obtained using the information available at the Global Volcanism Program (Global Volcanism Program, 2023).

Since the detection capability depends on the migration path (James et al., 2023), we consider some of the most common magma patterns found in volcanic edifices, such as vertical, lateral and inclined magma paths (Pinel and Jaupart, 2004; Gudmundsson, 2002, 2006; Acocella and Neri, 2009; Bistacchi et al., 2012; Rivalta et al., 2015; Tibaldi, 2015). Thus, in our analysis, we evaluate the detection capability for each volcano, accounting all these migration types, and consider how the proximity of a station to the vent influences the coverage of the central conduit area.

As a measure of the seismic network efficiency, we calculate the average detection capability volume per station and use the random forest regression algorithm (Pedregosa et al., 2011) to identify which statistical features of the seismic network influence more the efficiency. Notably, our findings indicate that optimizing seismic network coverage involves maximizing the standard deviation of distances between station pairs while also ensuring a minimum prescribed separation distance. We believe our results provide valuable information for smart seismic network design, particularly useful in crisis response scenarios and regions with limited resources, where maximizing the coverage of available monitoring stations is crucial.

Ideally, the seismic network optimization strategies to detect magma migrations using SARA should be implemented alongside with other design principles, that consider multiparametric analysis.

2. Methodology

2.1. SARA detection capability

The SARA method (Taisne et al., 2011), uses the seismic amplitude decay (Yamasato, 1997; Jolly et al., 2002; Battaglia and Aki, 2003), to calculate the mean seismic amplitude ratio (A_i) between a pair of seismic stations (i = 1,2):

$$\frac{A_1}{A_2} = \frac{r_2}{r_1} e^{-B(r_1 - r_2)} \tag{1}$$

Where r_i is the distance between the source and the station, the attenuation coefficient $B = (\pi f)/(Q\beta)$, with f the mean frequency, Q the quality factor, and β the shear-wave velocity (Aki and Richards, 1980). This equation is applicable for high-frequency isotropic body S-waves (Morioka et al., 2017) and offers the advantage of eliminating the dependence of the source seismic amplitude.

Eq. 1 can be used to calculate the hypocentres, if the seismic amplitude is corrected for instrument and site amplification factors (Taisne et al., 2011; Caudron et al., 2015, 2018). In crisis response scenarios, it can be used for real time seismic migration identification (Tan et al., 2019), by calculating the seismic amplitude Ai, as the envelope of a band passed seismic signal in a time window larger than the differential travel time (Taisne et al., 2011).

Following James et al., 2023, the seismic migrations could be identified only in the cases that the amplitude ratio changes along a migration path, are larger than the signal variability caused by seismic noise during the magma intrusion. In other words, for a seismic migration starting at $\boldsymbol{r} - \delta$, and finishing at $\mathbf{r}$ (or a migration moving in the opposite direction since we apply absolute value), there will be a positive detection in stations 1,2 if:

$$\Delta LAR_{1,2}(\boldsymbol{r}, \delta) = \left| \left| log\left(\frac{A_1(\boldsymbol{r})}{A_2(\boldsymbol{r})}\right) \right| - \left| log\left(\frac{A_1(\boldsymbol{r}-\delta)}{A_2(\boldsymbol{r}-\delta)}\right) \right| \right| \geq threshold \tag{2}$$

The '*threshold*' here represents the logarithm of the expected variability in the seismic signal. In James et al., 2023, it was calculated as the standard deviation of the detrended logarithm of the seismic amplitude in a real migration episode at Piton de la Fournaise (Tan et al., 2019; James et al., 2023), here we use the same parameter (0.1) in our calculations.

To establish a positive detection across the entire seismic network, it is crucial to ensure that ΔLAR changes correspond to actual migration events rather than localized phenomena (such as station malfunction or animal disruption). In a seismic network with n stations, each station forms n-1 pairs, so a localized event at one station can affect only n-1 pairs. To verify the independence of an event from any single station, we require ΔLAR changes to be observed in more than n-1 station pairs. Therefore, we establish the criterion that Eq. 2 must hold true for a minimum of n pairs of stations.

In summary, we use Eq. 2 and the above criteria, to calculate the volume under the volcanoes' surface, where we have positive detection i.e., the detection capability volume, hereafter referred to as the 'DCV'. As can be seen from the definition, the direction of the migration given by the vector δ, plays a major role in determining whether the migration can be detected. In the following section we will describe the seismic migration directions considered in our analysis.

2.2. Magma migrations directions

As magma propagates, it generates, or activates, fractures in the crust due to pressure build-up (Rubin, 1993). Subsequently, these fractures are filled by magma, forming dikes that propagate in a direction controlled by the stress field near the dike tip (Nakamura, 1977; Rubin and Gillard, 1998). Dike emplacement is highly sensitive to the particular characteristics of each volcano, since it is controlled by the interplay of magmatic forces, stiffness contrasts within the host rock (Gudmundsson, 2006; Kavanagh et al., 2006), the topography of the volcano (Tibaldi, 2003; Acocella and Neri, 2009; Rivalta et al., 2015), regional tectonic stresses (e.g., Paquet et al., 2007; Sigmundsson et al., 2015), and gravitational loading (Pinel and Jaupart, 2004; Münn et al., 2006; Roman and Jaupart, 2014; Maccaferri et al., 2017).

In this paper we consider >100 volcanoes with different topographies and tectonic settings. Developing a tailored model that describes magma migrations for each volcano falls beyond the scope of this paper. Instead, we focus on 3 migration directions, inspired by some of the most commonly observed dike patterns.

a) **Vertical migrations**. – Vertical magma propagation is predominantly driven by buoyancy (Pansino et al., 2023) and usually takes place within the central conduit area. Radial or peripheral dikes

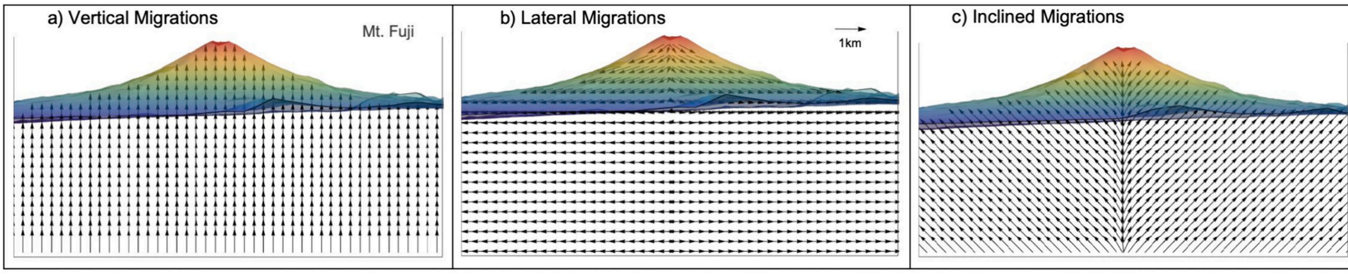

Fig. 1. Migration directions considered. In all cases the migrations are 1 km length. a) Vertical magma migration b) Lateral radial migrations- horizontal migrations below the volcano edifice and downslope migrations within the volcano edifice (for details on the dip angle function see appendix). C) Inclined radial migrations- with a 45degree angle respect the volcano axis. In B) and C) the volcano axis is defined as the vertical axis below the volcano's vent 'coordinates (Global Volcanism Program, 2023).

propagating vertically may appear if the main conduit is closed and/ or if magma is feed from a peripheral system (Acocella and Neri, 2003, 2009; Geshi, 2008). In our analysis, we consider vertical migrations starting anywhere below the volcano surface (Fig. 1-a).

b) **Lateral migrations**. –Radial dikes propagating laterally away from the volcano axis (defined here as the vertical axis below the volcano's vent), may appear due to local stress from the magma reservoir or volcano load (Pinel and Jaupart, 2004; Acocella and Neri, 2003, 2009; Kervyn et al., 2009; Roman and Jaupart, 2014). Also, rigidity layering, and the presence of topographic gradient can favor their formation (Urbani et al., 2018). Lateral dikes have been observed in many volcanoes (see Rivalta et al., 2015 for a review). In prominent volcanoes, they appear at the base and higher up, they extend downslope from the central conduit (Nakamura, 1977; Poland et al., 2008; Acocella and Neri, 2009). In this paper, we consider horizontal radial migrations starting anywhere below the volcanic edifice and radial downslope migrations within the edifice. For downslope migrations, we increment the dipping angle linearly with the volcano height (see Fig. 1-b and Appendix for details).

c) **Inclined migrations**: -. Radial inclined magma sheets ascending through the edifice toward the flanks, may appear due the interplay between the magma overpressure and the normal stress in the host rock, or/and as result of inflating shallow magma chambers (Gudmundsson, 2002; Galland et al., 2014; Harp and Valentine, 2018). They have been observed in eroded volcanic fields with a roughly conical orientation around the volcano axis (Gudmundsson, 2002; Bistacchi et al., 2012; Harp and Valentine, 2018; Geshi, 2008; Porreca et al., 2006). In our analysis we consider inclined radial migration starting anywhere below the volcano surface, with a 45-degree azimuthal angle with respect to the volcano axis (se Fig. 1-c).

To study the natural direction variability observed in real dikes, we incorporate random perturbations around the vertical migrations using Vesuvius volcano as a case of study, our aim is to test how this variability can affect the vertical detection capability volume (DCV-vertical). We performed 50 simulations for each 10-degree increment of perturbations to study this effect (see Appendix).

The length of all migration considered is 1 km long. Thus, 1 km is the minimum migration length that we consider for positive detection, any longer migration will also be detected within this volume, as the DCV increases with the migration length (James et al., 2023). Details about the exact mathematical model used to describe the migrations directions are given in the supplementary material.

2.3. Seismic networks and Topography data

In this analysis, we retrieve seismic station's locations from GVMID (Widiwijayanti et al., 2024) web site (https://wovodat.org/gvmid/home.php) and the Earth Scope Consortium (formerly IRIS and UNAVCO) web service *(https://service.iris.edu/)*, funded through the Seismological Facility for the Advancement of Geoscience (SAGE). We use seismic stations located within 15 km of the vent. The volcanic vents are located using the coordinates available at the GVP (Global Volcanism Program, 2023). These seismic stations might include both the

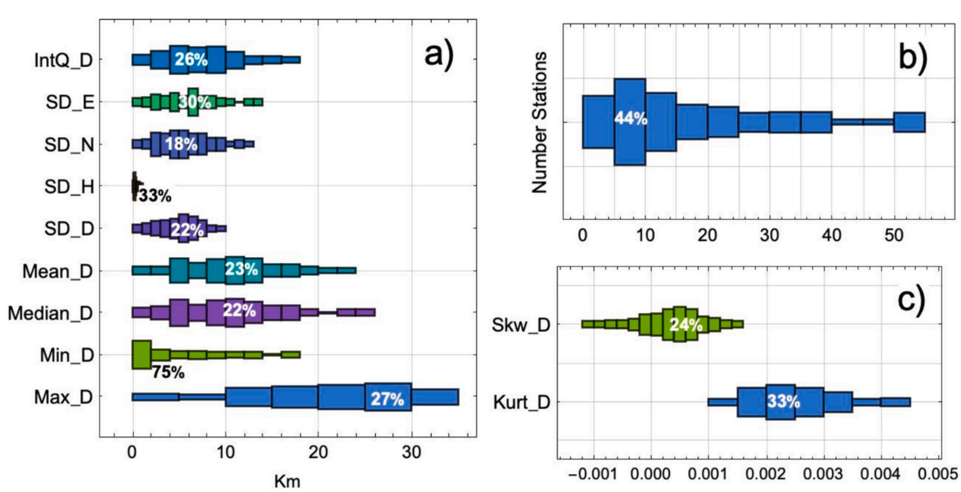

Fig. 2. Histogram of the statistical features of the 116 seismic networks analyzed. IntQ stands for Interquartile range, SD stands for standard deviation, Skw = Skewness and Kurt = Kurtosis. E = Eastings coordinates of stations, N=Northing coordinates of stations, H=Height coordinates of stations. D = distance between station pairs in the network.

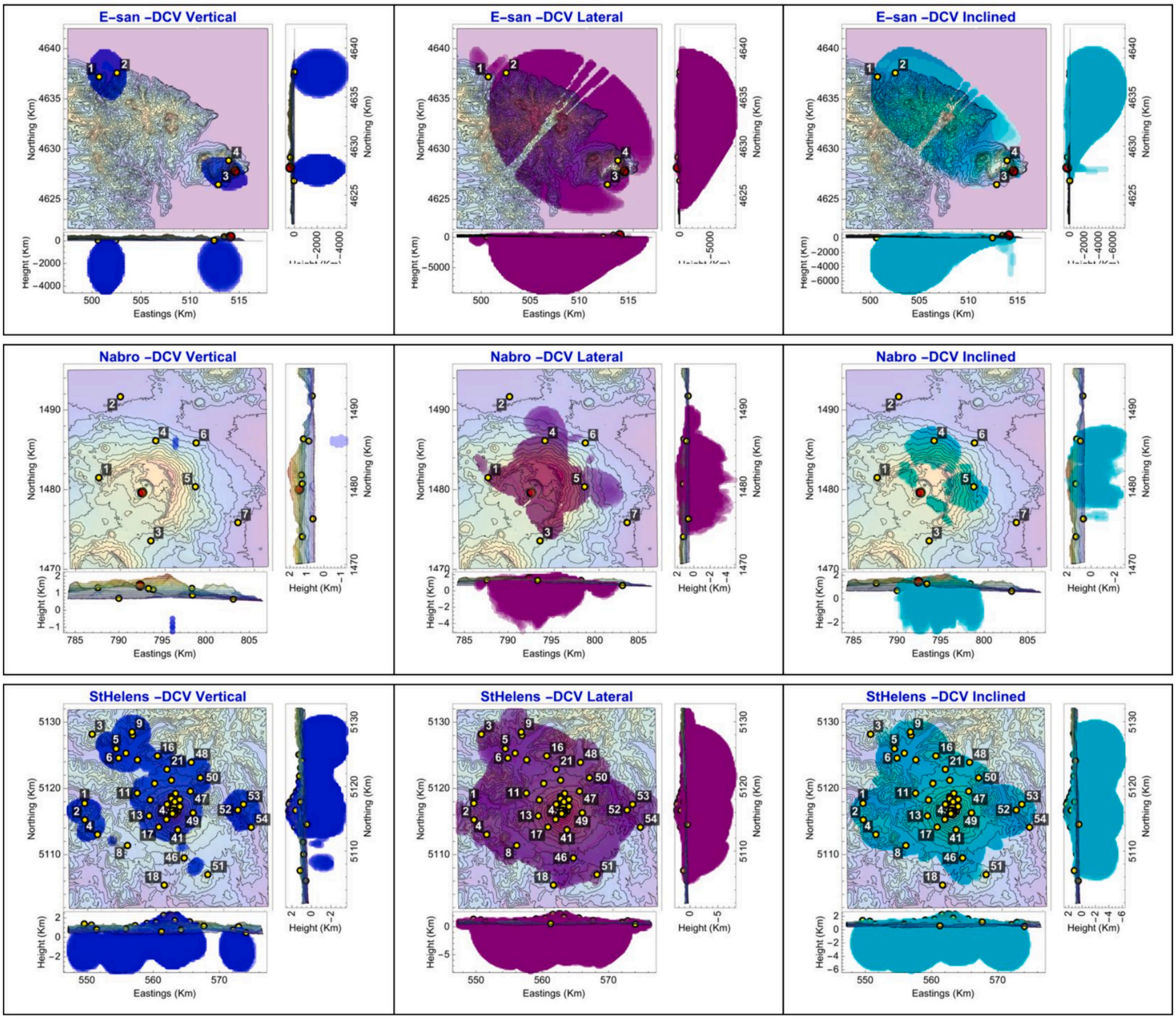

Fig. 3. First Row- Detection Capability Volume (DCV) for E-San. Second row- DCV for Nabro. Third Row- DCV for St. Helens. The first column is for vertical migrations, the second for lateral migrations and the third for Inclined migrations as explained in Fig. 1. The location of the seismic stations is label with numbers, their coordinates are given in the supplementary material. The decay coefficient in Eqs. 1 and 2 is B = $1.087*10^{-4}$. The location of the seismic stations labelled with numbers is given in the complementary material.

volcano monitoring seismic network and stations from larger seismic networks that monitor tectonic seismic events. We used stations whose “operation end date” in the database is in the future or is unknown, and thus might be active, although there is the possibility that this information is not updated for all stations and some of the seismic stations were part of temporal deploys. Hence, we don’t pretend to make an up-to-date assessment of volcanoes seismic networks, but rather use the seismic network data available to study real case scenarios that can help us to draw conclusions on optimal seismic network design for using the SARA algorithm.

We analyzed a total of 116 volcanoes, classified as stratovolcanoes, caldera, pyroclastic shield, complex volcano, lava dome, shield volcano, pyroclastic cone, fissure vent and somma volcano. About 44% of the seismic networks have between 5 and 10 stations as can be seen in the histogram in Fig. 2-b. Also, the arithmetic mean and median distance between station pairs in the seismic network analyzed is on the 10’s of km. We also plot other statistical features of the distribution of the seismic networks analyzed, that show the diversity of the seismic network’s arrays. The topography of the terrain in each case was obtained using the SRTM data (Rabus et al., 2003; Farr et al., 2007), via the Earth Explorer website (https://earthexplorer.usgs.gov/). This information is used to delimit the volume where magma migrations can appear and hence is the boundary of our calculations.

3. Results

3.1. Assessment of the seismic network coverage

In Fig. 3 we present the DCV for vertical, lateral and inclined migrations at E-san (Japan), Nabro (Eritrea) and St. Helens (U.S.A) volcano, the plots for the rest of the volcanoes are in the supplementary material. The DCV represents the volume where we could detect 1 km or longer migrations in the given directions, as the change of the SARA (given by Eq. 2), would be above the estimated variability of the seismic source path. In all the volcanoes analyzed, we found that the DCV is greater for lateral and inclined migrations compared to vertical migrations.

We further study how random magma migration directions can

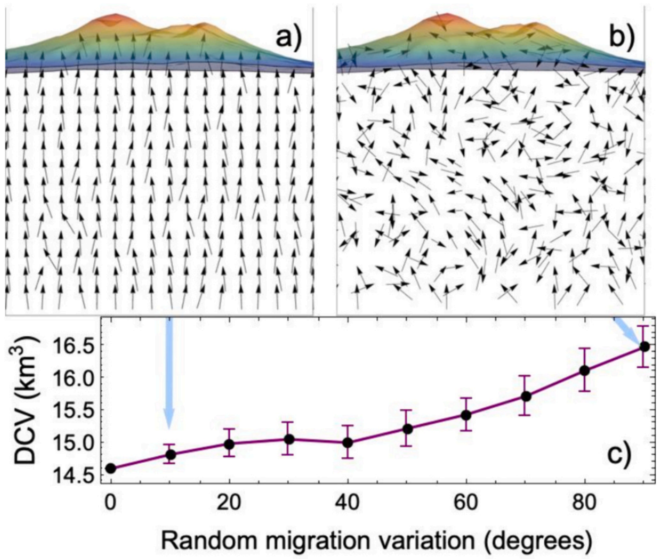

Fig. 4. Perturbations of vertical magma migration directions a) varying randomly in the [−10,10] degrees range. b) Same as but varying randomly the azimuth angle in the [−90,90] degrees range. c) Change in the DCV for different perturbations in the migration direction. Each dot is the average of 50 simulations with the uncertainty given by the standard deviation of the results.

impact the DCV. We study this effect only in Vesuvius volcano. We increase gradually the perturbations, as shown in Fig. 4; the first point at 0 correspond to vertical migration with no perturbations; the next point at 10 degrees corresponds to the mean of 50 simulations where we vary randomly the azimuth angle respect to the vertical axis in the [−10,10] degree range (see Fig. 4 a), and so forth, until we vary randomly the azimuth angle in the [−90,90] range.

As is shown in Fig. 4 we found that, for small perturbations the detection volume doesn't change significantly, but as we increase the perturbations including more wide-spread magma migration directions (Fig. 4 b), the detection volume increases. This confirm that SARA could be more effective at detecting lateral or inclined magma migrations over vertical migrations.

Also, we observed a great variation of the detection capability volume compared to the number of stations. In general, the detection capability volume increases roughly with the number of stations as shown in Fig. 5, but there are many exceptions, see for instance, *E*-san volcano with 4 stations, and Nabro with 7, in this case the former has a higher detection capability despite having fewer stations (see Fig. 3). We also show St. Helens volcano, which has one of the best coverages around the summit due to its dense seismic network array close to the conduit (54 stations); however, this large seismic network array is likely composed of many temporal stations that could be deployed for short term projects.

3.1.1. *Volcanic conduit coverage*

We calculated the volcanic conduit coverage ratio for vertical migrations, which are the most relevant in this area.

For the volcanoes considered in our calculations, the maximum depth of the detection capability volume (relative to the vent height), ranges between 2 and 10 km depth (see mp4 in supplementary material), with a mean of approximately 6 km. However, the depth of detectability below the vent is usually less than this maximum value. Thus, to estimate the conduit coverage, we defined the conduit volume as the volume within a cylinder centred in the volcanic axis with a 500 m radius and 5 km depth (I.e., 5 km depth below the volcano's vent given by GVP). Then calculated the fraction of grid points displaying positive detection within this volume (see Fig. 6). In other words, the "conduit coverage ratio", is defined as the ratio between the total conduit volume and the volume in which the migration is detectable. Consequently, a conduit coverage ratio of one, represents a total coverage for vertical migrations in this volume.

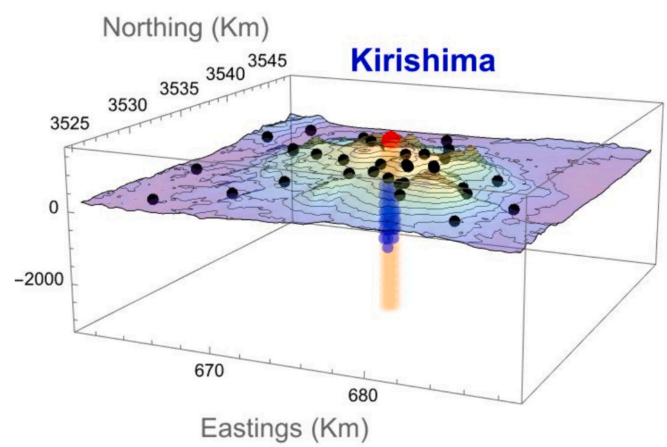

Fig. 6. Kirishima's conduit coverage. The seismic stations are indicated with black dots. The vent is indicated with a red dot and below it the central conduit defined as the area within a 500 m radius and 5 km depth (light red dots). The blue dots indicate where there is positive detection in the central conduit for 1 km vertical migrations.

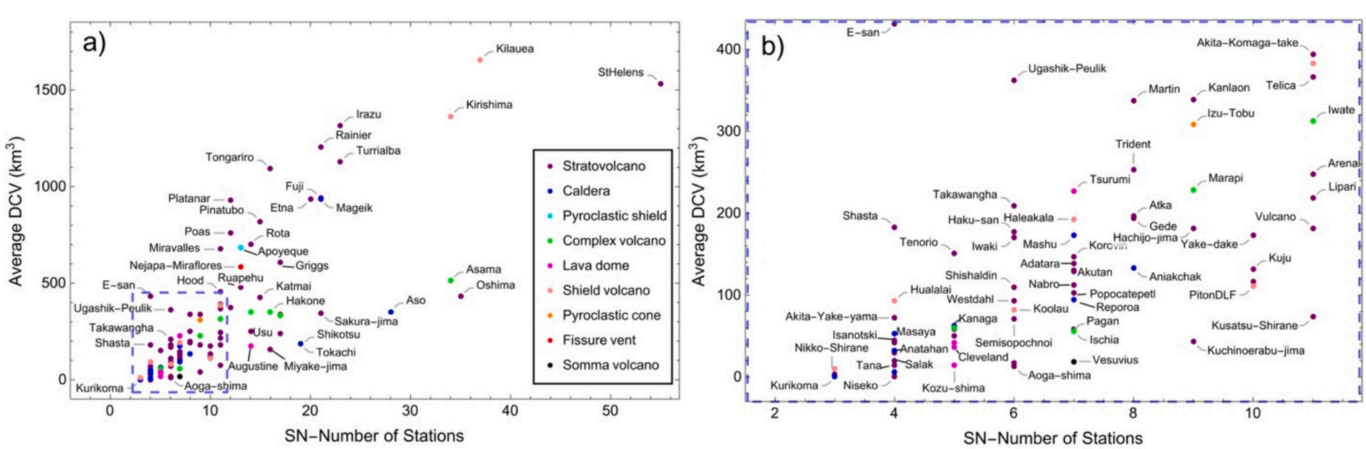

Fig. 5. a) Average detection volume capability (sum of vertical, lateral and inclined DCV divided by 3) as a function of the number of seismic stations for each seismic network. b) zoom-in on figure a).

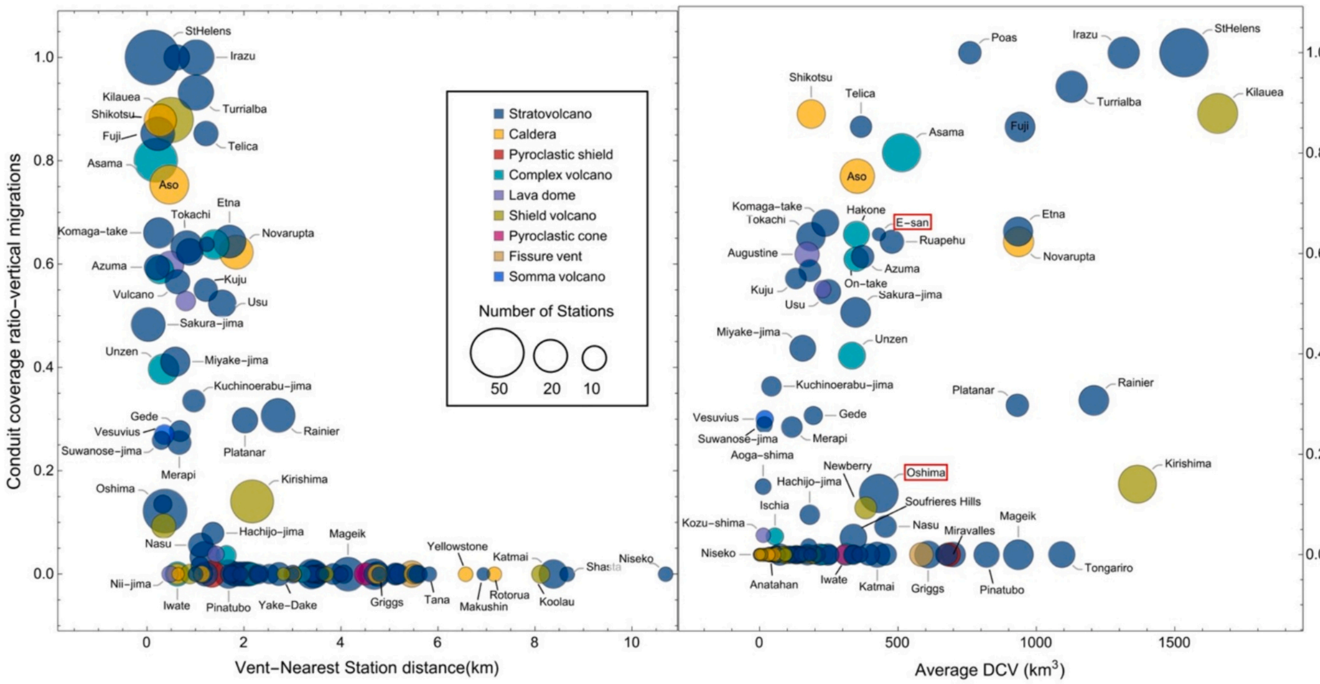

Fig. 7. a) Conduit coverage ratio vs the distance between the vent and its closest seismic station for different volcanoes. B) Conduit coverage ratio vs the Average DCV. The size of the circles is proportional to the number of seismic stations in the volcano's network. 'Oshima' and '*E*-san' labels in figure b are highlighted to guide the reader in further discussion.

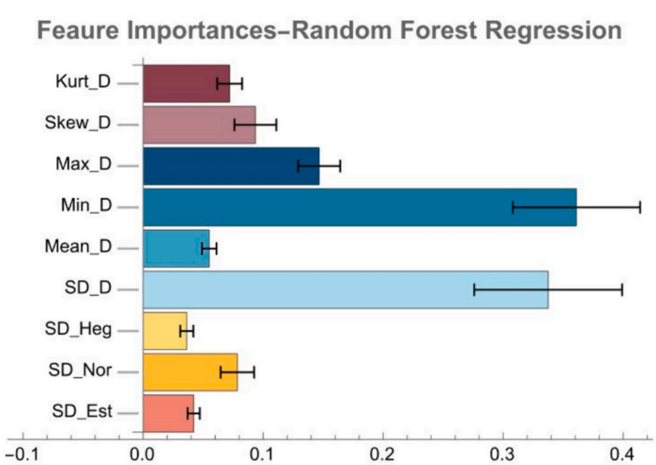

Fig. 8. Determination of feature importance for enhancing the detection capability volume, carried out through the random forest regression algorithm. We include as features the Maximum (Max), Minimum (Min), Mean, Standard deviation (SD), Skewness (Skew) and Kurtosis (Kurt) of the distance between station pairs (D). Also, the SD of the seismic network height (DH), northings (DN) and eastings (DE) coordinates. The Median and Interquartile range features were discarded as for our samples these were highly correlated to the Mean and Standard deviation respectively.

We found that a good conduit coverage is closely related to the location of the seismic stations. In Fig. 7-a, we show that volcanoes with conduit coverage ~1 have seismic stations located within a 2 km distance from the vent. Nevertheless, we observe this condition is necessary but not sufficient, as we also have many examples of other volcanoes with seismic stations close to the vent, but with poor conduit coverage.

In Fig. 7-b we plotted the overall detection coverage, considering both the conduit coverage and the average detection capability volume, including vertical, lateral and inclined seismic migrations; the best coverage corresponds to volcanoes located at the top right corner of the figure. As we can see, the relation between seismic network size and detection capability volume is variable, for instance, *E*-san and Oshima, have about the same average detection capability volume but Oshima network is much larger than E-san. Thus, if we consider the efficiency as the average detection capability volume divided by the number of seismic stations, we infer that there are some seismic networks that are more efficient than others.

3.2. *Seismic network efficiency*

To estimate which statistical properties of the seismic network's locations, impact more the efficiency, we use the random forest regression algorithm (Pedregosa et al., 2011). This algorithm allows us to quantify the contribution of individual input features in a model's predictive performance or output (see Appendix for details). Here, as an input, we use the uncorrelated statistic features of the seismic network location and as an output we use network's efficiency (average detection capability volume per station).

In Fig. 8 we present the impact that the seismic network statistical features, Fig. 2, have on the efficiency. As can be appreciated, the most relevant features are the standard deviation and by extension interquartile range, as well as, the minimum distance between stations pairs, this result was consistent using other parameters for the calculations, where these two features always stand out (see discussion for details). In a lesser degree, the maximum distance between station pairs is also a relevant parameter, the rest of the features have similar importance.

In order to inspect further the relation of these characteristics of the seismic network, in Fig. 9 we plot the top three features versus the average detection capability per station. We found that very sparse seismic networks, as defined by a minimum distance between station pair larger than about 7 km, red dots Fig. 9, have a low or zero detection capability, in Fig. 9-a. Also, we observe an increment of the average detection capability as we increase the standard deviation and the maximum distance between station pairs. This tendency can be clearly appreciated in Figs. 9-b and 9-c. One case that standout is E-San volcano, that has the highest average detection capability per station.

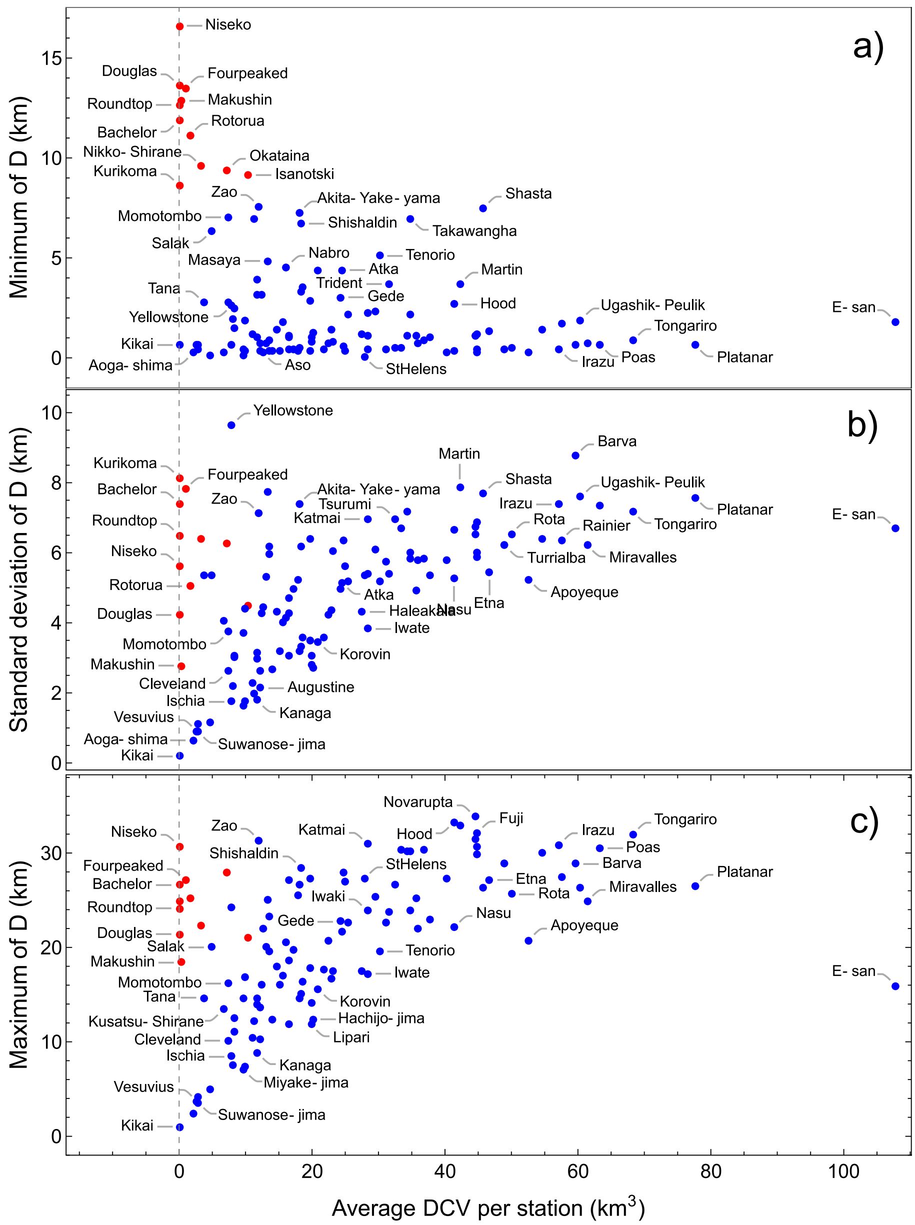

Fig. 9. We plot the statistical features of the seismic network and compare them to the average detection volume per station. In a) the vertical axis is the Minimum of the distance between stations pairs (D), in b) we plot the Standard deviation of D c) we plot the Maximum of D. The red dots are the volcanoes that have a large (>7.5 km) distance between station pairs. (For interpretation of the references to colour in this figure legend, the reader is referred to the web version of this article.)

4. Discussion

Our method to calculate the detection capability volume is based on Eqs. 1 and 2, that are valid under certain assumptions. Eq. 1 is valid for high frequency, isotropic radiating body-waves (Hofstetter and Malone 1986; Jolly et al., 2002; Morioka et al., 2017), this holds in volcanoes with high heterogeneous media, mean free paths $\leq 1km$ and strong intrinsic attenuation (Kumagai et al., 2011; Morioka et al., 2017). The quality factor Q, inversely proportional to energy attenuation, depends on the structural characteristics of volcanoes. For the high-frequency band, the value of Q has been estimated to range between 10 and 200 in various volcanoes (see Kumagai et al., 2020 and references therein). Additionally, within the same volcano, this factor can also vary with the depth. In Figs. 3–9 we used the same attenuation coefficient B=1.087*10^{-4}, for all the volcanoes, however we reproduced the calculations for other attenuation coefficients: 1.4x10^{-4} and 0.9x10^{-4}; for a frequency of ~10 Hz and a shear-wave velocity β = 1700 m/s (Aki and Richards, 1980), the Q factor falls in the [130−200] range. We observed that increasing the attenuation coefficient increases the DCV. Despite the attenuation coefficient being a rough approximation of realistic values for each volcano, utilizing a consistent attenuation value for all the volcanoes enabled us to effectively compare the detection capabilities based solely on seismic station locations.

To define a positive detection we used Eq. 2, where we compare two points in space assuming that magma migration is between these two locations. Nevertheless, the head of the dike can generate, or activate, fractures in an area around its tip (Rubin and Gillard, 1998), introducing some localized micro seismicity. This and other sources of seismic noise can vary from volcano to volcano, making the ideal '*threshold*' value in Eq. 2 different for each case. In James et al., 2023 it was demonstrated that increasing the threshold (for signals with higher noise) reduces the detection capability volume, thus if we would select a different value for the threshold, it would affect the detection capability volume for all the volcanoes.

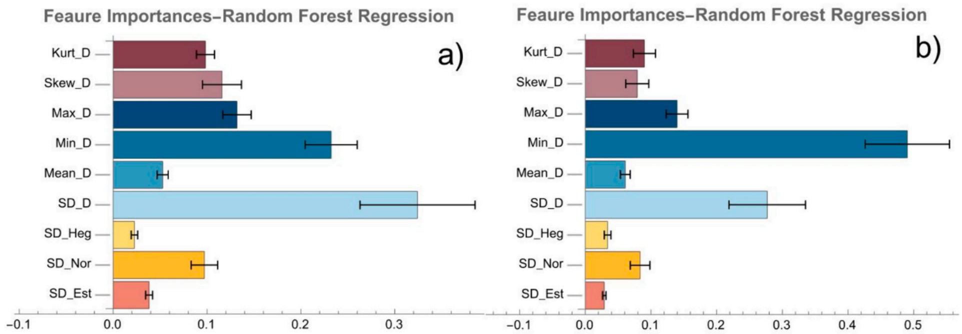

Fig. 10. Feature importance for different decay coefficients in Eq.1, for different attenuation coefficients. In a) B $= 1.4\mathrm{x}10^{-4}$and b) for B $= 0.9\mathrm{x}10^{-4}$.

In our analysis we used 3 seismic migration directions, vertical, radial lateral and radial inclined. However, there are other dike patterns that can be found in volcanoes that were not considered here, such as regional and circumferential dikes. Volcanoes located in strong regional tectonic settings are dominated by magma migrations oriented along the tectonic stress controlling dikes orientation, while circumferential dikes can appear due a pressurized magma reservoir and/or the load of the volcano (Acocella and Neri, 2009). Nevertheless, the primary control of dike propagation is the topographic relief, that produces radial dikes (Acocella and Neri, 2009) and were considered in our analysis. Also, although, we used the same migration directions for all the volcanoes, lateral migrations are perhaps more relevant for prominent volcanoes where the edifice load is important (Gudmundsson, 2002; Acocella and Neri, 2003; Pinel and Jaupart, 2004). Our results indicate that the detection capability volume is larger for radial propagating migration compared to vertical migration. This finding confirm that the gradient of the SARA (Eq.1) favours the detection of radially propagating migrations as speculated in James et al., 2023.

We analyzed the efficiency of the seismic networks to detect 1 km or longer migrations in the 3 directions described previously, by calculating the average detection capability volume per station. Then used the random forest regression algorithm to estimate the impact that the statistical properties of the seismic network have on the detection efficiency. This algorithm uses a stochastic analysis to determine the relevance of the input features (Pedregosa et al., 2011). Thus, we performed 500 runs for each attenuation coefficient and present the mean values in Fig. 10 with its respective errors. Also, we repeated the calculations for different attenuation coefficients, and we consistently observed that the standard deviation distance and the minimal distance between station pairs had the highest impact on efficiency (see Fig. 10). It must be noted, that in our calculations we used volcanoes with different topographies, however most of the volcano's considerer in our study are stratovolcanoes, and thus our results might by bias toward this volcano type.

Finally, the method of seismic network location optimization we discuss here focus solely on seismic migration detection using SARA and it doesn't consider other algorithms of optimization that involve hypocentre location, seismic imaging, source mechanism identification or others (Kijko, 1977; Hardt and Scherbaum, 1994; Tramelli et al., 2013; Toledo et al., 2020). Thus, to consider a multipurpose seismic network design, our results most be considered together with other important general guidelines that consider other objectives, as for instance, locating the seismic array in an area where the azimuthal gap (i. e. the largest gap in azimuth between stations seen from the epicentre) is <180 degrees (Valtonen et al., 2013) for hypocentre location; or consider average interspacing distance of the order of the expected hypocentres depths (Toledo et al., 2020).

5. Conclusions

We studied the optimal location of seismic networks for the detection of magma migrations exceeding 1 km using SARA. Our results suggest that SARA is more efficient detecting lateral and inclined magma migrations. Also, we found that to have a bigger detection coverage of vertical magma migrations around the volcanic conduit, it is necessary, though not sufficient, to have at least a seismic station within a 2 km radius from the vent. Furthermore, we demonstrated that the efficiency to detect vertical, lateral, and inclined seismic migrations can be enhanced by designing seismic networks with inter station pairs distance that exhibit a high standard deviation, while maintaining a minimum distance below 7 km.

In other words, the optimal spatial configuration for detecting magma migrations exceeding 1 km, is an irregular seismic stations array that has a minimum distance between station pairs below 7 km and has at least one station within 2 km from the vent.

As future work, our findings on seismic network design could be integrated with other seismic methods to explore optimal network locations that balance multiple objectives.

Supplementary data to this article can be found online at https://doi.org/10.1016/j.jvolgeores.2024.108138.

CRediT authorship contribution statement

T. Espinosa-Ortega: Writing – review & editing, Writing – original draft, Methodology, Investigation, Formal analysis, Data curation, Conceptualization. **B. Taisne:** Writing – review & editing, Writing – original draft, Supervision, Project administration, Methodology, Funding acquisition, Conceptualization.

Declaration of competing interest

The authors declare that they have no known competing financial interests or personal relationships that could have appeared to influence the work reported in this paper.

Data availability

The data used is shared in the supplementary material

Acknowledgement

This research/project is supported by the National Research Foundation, Singapore under its 8th NRF Investigatorship (NRFI) (Award NRF-NRFI08-2022-0015). This work comprises EOS contribution number 571.

References

Acocella, V., Neri, M., 2003. What makes flank eruptions? The 2001 Etna eruption and its possible triggering mechanisms. Bull. Volcanol. 65 (7), 517–529. https://doi.org/10.1007/s00445-003-0280-3.

Acocella, V., Neri, M., 2009. Dike propagation in volcanic edifices: Overview and possible developments. Tectonophysics 471 (1–2), 67–77. https://doi.org/10.1016/j.tecto.2008.10.002.

Aki, K., Richards, P., 1980. Quantitative Seismology: Theory and Methods, vol. I. W.H. Freeman, New York, p. 557. https://doi.org/10.1002/gj.3350160110.
Battaglia, J., Aki, K., 2003. Location of seismic events and eruptive fissures on the Piton de la Fournaise volcano using seismic amplitudes. J. Geophys. Res. 108 (B8), 2364. https://doi.org/10.1029/2002JB002193.
Bistacchi, A., Tibaldi, A., Pasquarè, F.A., Rust, D., 2012. The association of cone–sheets and radial dykes: Data from the Isle of Skye (UK), numerical modelling, and implications for shallow magma chambers. Earth Planet. Sci. Lett. 339–340 (2012), 46–56. https://doi.org/10.1016/j.epsl.2012.05.020.
Caudron, C., Taisne, B., Kugaenko, Y., Saltykov, V., 2015. Magma migration at the onset of the 2012-13 Tolbachik eruption revealed by Seismic Amplitude Ratio Analysis. J. Volcanol. Geotherm. Res. 307, 60–67. https://doi.org/10.1016/j.jvolgeores.2015.09.010.
Caudron, C., White, R.S., Green, R.G., Woods, J., Ágústsdóttir, T., Donaldson, C., Greenfield, T., Rivalta, E., Brandsdóttir, B., 2018. Seismic amplitude ratio analysis of the 2014–2015 Bár ∂arbunga-Holuhraun dike propagation and eruption. J. Geophys. Res. Solid Earth 123, 264–276. https://doi.org/10.1002/2017JB014660.
Chouet, B., 1996. Long-period volcano seismicity: its source and use in eruption forecasting. Nature 380, 309–316. https://doi.org/10.1038/380309a0.
Costa, F., Widiwijayanti, C., Win, N.T.Z., Fajiculay, E., Espinosa-Ortega, T., Newhall, C. G., 2019. WOVOdat – the global volcano unrest database aimed at improving eruption forecasts. Disaster Prev Manag 28 (6), 738–751. https://doi.org/10.1108/DPM-09-2019-0301.
Curtis, A., 1999. Optimal experiment design: cross-borehole tomographic examples. Geophys. J. Int. 136 (3), 637–650. https://doi.org/10.1046/j.1365-246x.1999.00749.x.
Eibl, E., Bean, C.J., Vogfjörd, K., Braiden, A., 2014. Persistent shallow background micro seismicity on Hekla volcano, Iceland: a potential monitoring tool. J. Volcanol. Geotherm. Res. 289, 224–237. https://doi.org/10.1016/j.jvolgeores.2014.11.004.
Eibl, E., Bean, C.J., Vogfjörd, K.S., Ying, Y., Lokmer, I., Möllhoff, M., O'Brien, G.S., 2017. Tremor-rich shallow dyke formation followed by silent magma flow at Bárðarbunga in Iceland. Nat. Geosci. 10 (4), 299–304. https://doi.org/10.1038/ngeo2906.
Ewert, J.W., Guffanti, Marianne, Murray, T.L., 2005. An assessment of volcanic threat and monitoring capabilities in the United States: Framework for a National Volcano Early Warning. System: U.S. Geological Survey Open-File Report 2005-1164 62. https://pubs.usgs.gov/publication/ofr20051164.
Farr, T.G., et al., 2007. The shuttle Radar Topography Mission. Rev. Geophys. 45, RG2004. https://doi.org/10.1029/2005RG000183.
Galland, O., Burchardt, S., Hallot, E., Mourgues, R., Bulois, C., 2014. Dynamics of dikes versus cone sheets in volcanic systems. J. Geophys. Res. Solid Earth 119, 6178–6192. https://doi.org/10.1002/2014JB011059.
Geshi, N., 2008. Vertical and lateral propagation of radial dikes inferred from the flow-direction analysis of the radial dike swarm in Komochi Volcano, Central Japan. J Volcanol Geotherm Res 173 (1–2), 122–134. https://doi.org/10.1016/j.jvolgeores.2008.01. 001.
Global Volcanism Program, 2023. [Database] Volcanoes of the World (v. 5.1.5; 15 Dec 2023). Distributed by Smithsonian Institution, compiled by Venzke, E. https://doi.org/10.5479/si.GVP.VOTW5-2023.5.1.
Gudmundsson, A., 2002. Emplacement and arrest of sheets and dykes in central volcanoes. J. Volcanol. Geotherm. Res. 116 (3–4), 279–298. https://doi.org/10.1016/S0377-0273(02)00226-3.
Gudmundsson, A., 2006. How local stresses control magma-chamber ruptures, dyke injections, and eruptions in composite volcanoes. Earth Sci. Rev. 79 (1–2), 1–31. https://doi.org/10.1016/j.earscirev.2006.06.006.
Hardt, M., Scherbaum, F., 1994. The design of optimum networks for aftershock recordings. Geophys. J. Int. 6 https://doi.org/10.1111/j.1365-246X.1994.tb02464.x.
Harp, A.G., Valentine, G.A., 2018. Emplacement controls for the basaltic-andesitic radial dikes of Summer Coon volcano and implications for flank vents at stratovolcanoes. Bull. Volcanol. 80, 16. https://doi.org/10.1007/s00445-018-1194-4.
Hofstetter, A., Malone, S.D., 1986. Observations of volcanic tremor at Mount St. Helens in April and May 1980. Bulletin of the Seismological Society of America 76 (4), 923–938.
James, K.E., Espinosa-Ortega, T., Tan, C.T., Taisne, B., 2023. Assessing the potential to detect vertical magma migration using seismicity through the analysis of the seismic network design. J. Volcanol. Geotherm. Res. 435, 107769 https://doi.org/10.1016/j.jvolgeores.2023.107769.
Jolly, A., Thompson, G., Norton, G., 2002. Locating pyroclastic flows on Soufriere Hills volcano, Montserrat, West Indies, using amplitude signals from high dynamic range instruments. J. Volcanol. Geotherm. Res. 118, 299–317. https://doi.org/10.1016/S0377-0273(02)00299-8.
Kavanagh, J.L., Menand, T., Sparks, R.S.J., 2006. An experimental investigation of sill formation and propagation in layered elastic media. Earth Planet. Sci. Lett. 245, 799–813. https://doi.org/10.1016/j.epsl.2006.03.025.
Kervyn, M., Ernst, G.G.J., van Wyk, B., de Vries, L., Jacobs, P., 2009. Volcano load control on dyke propagation and vent distribution: Insights from analogue modelling. J. Geophys. Res. 114, B03401. https://doi.org/10.1029/2008JB005653.
Kijko, A., 1977. An algorithm for the optimal distribution of a regional seismic network — I. Pure and Applied Geophysics 115, 999–1009. https://link.springer.com.remotexs.ntu.edu.sg/article/10.1007/BF00881222.
Kumagai, H., Nakano, M., Maeda, T., Yepes, H., Palacios, P., Ruiz, M., Arrais, S., Vaca, M., Molina, I., Yamashima, T., 2010. Broadband seismic monitoring of active volcanoes using deterministic and stochastic approaches. J. Geophys. Res. 115, B08303. https://doi.org/10.1029/2009JB006889.
Kumagai, H., Saito, T., O'Brien, G., Yamashina, T., 2011. Characterization of scattered seismic wavefields simulated in heterogeneous media with topography. J. Geophys. Res. 116, B03308. https://doi.org/10.1029/2010JB007718.
Kumagai, H., Lacson, R., Maeda, Y., Figueroa, M.S., Yamashina, T., Ruiz, M., Palacios, P., Ortiz, H., Yepes, H., 2013. Source amplitudes of volcano-seismic signals determined by the amplitude source location method as a quantitative measure of event size. J. Volcanol. Geotherm. Res. 257, 57–71.
Kumagai, H., Londoño, J.M., Maeda, Y., Acevedo Rivas, A.E., 2019. Amplitude source location method with depth-dependent scattering and attenuation structures: Application at Nevado del Ruiz volcano, Colombia. J. Geophys. Res. Solid Earth 124, 11585–11600. https://doi.org/10.1029/2019JB018156.
Kumagai, H., Torres, R., Maeda, Y., 2020. Scattering and attenuation characteristics at volcanoes inferred from envelope widths of natural and active seismic sources. Journal of Geophysical Research: Solid Earth 125 (11), e2020JB020249.
Kurokawa, A., Takeo, M., Kurita, K., 2016. Two types of volcanic tremor changed with eruption style during 1986 Izu-Oshima eruption. J. Geophys. Res. Solid Earth 121, 2727–2736. https://doi.org/10.1002/2015JB012500.
Lahr, J.C., Chouet, B.A., Stephens, C.D., Power, J.A., Page, R.A., (1994). Earthquake classification, location, and error analysis in a volcanic environment: Implications for the magmatic system of the 1989–1990 eruptions at Redoubt volcano, Alaska. J. Volcanol. Geotherm. Res. 62, 137–151. https://doi.org.remotexs.ntu.edu.sg/10.1016/0377-0273(94)90031-0.
Lanza, F., Waite, G.P., 2018. A nonlinear approach to assess network performance for moment-tensor studies of long-period signals in volcanic settings. Geophys. J. Int. 215 (2), 1352–1367. https://doi.org/10.1093/gji/ggy338.
Maccaferri, F., Richter, N., Walter, T.R., 2017. The effect of giant lateral collapses on magma pathways and the location of volcanism. Nat. Commun. 8, 1097. https://doi.org/10.1038/s41467-017-01256-2.
Maurer, H., Nuber, A., Martiartu, N., Reiser, F., Boehm, C., Manukyan, E., Schmelzbach, C., Fichtner, A., 2017. Optimized experimental design in the context of seismic full waveform inversion and seismic waveform imaging. Adv. Geophys. 58, 1–45. https://doi.org/10.1016/bs.agph.2017.10.001.
McNutt, S.R., 1994. Volcanic tremor amplitude correlated with eruption explosivity and its potential use in determining ash hazards to aviation. U.S. Geol. Survey Bull. 2047, 377–385.
Miller, C.A., Jolly, A.D., 2014. A model for developing best practice volcano monitoring: a combined threat assessment, consultation and network effectiveness approach. Nat. Hazards 71, 493–522. https://doi.org/10.1007/s11069-013-0928-z.
Morioka, H., Kumagai, H., Maeda, T., 2017. Theoretical basis of the amplitude source location method for volcano-seismic signals. J. Geophys. Res. Solid Earth 122, 6538–6551. https://doi.org/10.1002/2017JB013997.
Münn, S., Walter, T.R., Klügel, A., 2006. Gravitational spreading controls rift zones and flank instability on El Hierro, Canary Islands. Geol. Mag. 143, 257–268. https://doi.org/10.1017/S0016756806002019.
Nakamura, K., 1977. Volcanoes as possible indicators of tectonic stress orientation: principle and proposal. J. Volcanol. Geotherm. Res. 2, 1–16.
Newhall, C.G., Costa, F., Ratdomopurbo, A., Venezky, D.Y., Widiwijayanti, C., Win, N.T. Z., Tan, K., Fajiculay, E., 2017. WOVOdat – an online, growing library of worldwide volcanic unrest. J. Volcanol. Geotherm. Res. 345, 184–199. ISSN 0377-0273,. https://doi.org/10.1016/j.jvolgeores.2017.08.003.
Ogiso, M., Yomogida, K., 2021. Estimation of relative source locations from seismic amplitude: application to earthquakes and tremors at Meakandake volcano, eastern Hokkaido, Japan. Earth Planets Space 73, 29. https://doi.org/10.1186/s40623-021-01366-8.
Pansino, S., Emadzadeh, A., Taisne, B., 2023. Magma flow patterns in dikes: Observations from analogue experiments. Journal of Geophysical Research: Solid Earth 128. https://doi.org/10.1029/2022JB025463 e2022JB025463.
Pedregosa, F., Varoquaux, G., Gramfort, A., Michel, V., Thirion, B., Grisel, O., Blondel, M., Prettenhofer, P., Weiss, R., Dubourg, V., Vanderplas, J., Passos, A., Cournapeau, D., Brucher, M., Perrot, M., Duchesnay, E., 2011. Scikit-learn: Machine Learning in Python. J. Mach. Learn. Res. 12, 2825–2830.
Pinel, V., Jaupart, C., 2004. Magma storage and horizontal dyke injection beneath a volcanic edifice. Earth Planet. Sci. Lett. 221 (1–4), 245–262. https://doi.org/10.1016/S0012-821X(04)00076-7.
Poland, M.P., Moats, W.P., Fink, J.H., 2008. A model for radial dike emplacement in composite cones based on observations from Summer Coon volcano, Colorado, USA. Bull. Volcanol. 70, 861–875. https://doi.org/10.1007/s00445-007-0175-9.
Porreca, M., Acocella, V., Massimi, E., Mattei, M., Funiciello, R., De Benedetti, A.A., 2006. Geometric and kinematic features of the dike complex at Mt. Somma, Vesuvio (Italy). Earth Planet. Sci. Lett. 245 (1–2), 389–407. https://doi.org/10.1016/j.epsl.2006.02.027.
Paquet, F., Dauteuil, O., Hallot, E., Moreau, F., 2007. Tectonics and magma dynamics coupling in a dyke swarm of Iceland. Journal of Structural Geology 29 (9), 1477–1493. https://doi.org/10.1016/j.jsg.2007.06.001.
Rabus, B., Eineder, M., Roth, A., Bamler, R., 2003. The shuttle radar topography mission-a new class of digital elevation models acquired by spaceborne radar. Photogramm. Rem. Sens. 57, 241–262. https://doi.org/10.1016/S0924-2716(02)00124-7.
Rivalta, E., Taisne, B., Bunger, A.P., Katz, R.F., 2015. A review of mechanical models of dike propagation: Schools of thought, results and future directions. Tectonophysics 638 (2015), 1–42. https://doi.org/10.1016/j.tecto.2014.10.003.
Roman, A., Jaupart, C., 2014. The impact of a volcanic edifice on intrusive and eruptive activity. Earth Planet. Sci. Lett. 408, 1–8. https://doi.org/10.1016/j.epsl.2014.09.016.
Rubin, A.M., 1993. Tensile fracture of rock at high confining pressure: implications for dike propagation. J. Geophys. Res. 98, 15919. https://doi.org/10.1029/93JB01391.

Rubin, A.M., Gillard, D., 1998. Dike-induced earthquakes: theoretical considerations. J. Geophys. Res. 103, 10,017–10,030. https://doi.org/10.1029/97JB03514.

Sigmundsson, F., Hooper, A., Hreinsdóttir, S., Vogfjörd, K.S., Ófeigsson, B.G., Heimisson, E.R., Dumont, S., Parks, M., Spaans, K., Gudmundsson, G.B., Drouin, V., Árnadóttir, T., Jónsdóttir, K., Gudmundsson, M.T., Högnadóttir, T., Fridriksdóttir, H. M., Hensch, M., Einarsson, P., Magnússon, E., Samsonov, S., Brandsdóttir, B., White, R.S., Ágústsdóttir, T., Greenfield, T., Green, R.G., Hjartardóttir, ÁR., Pedersen, R., Bennett, R.A., Geirsson, H., La Femina, P.C., Björnsson, H., Pálsson, F., Sturkell, E., Bean, C.J., Möllhoff, M., Braiden, A.K., Eibl, E.P., 2015. Segmented lateral dyke growth in a rifting event at Bárðarbunga volcanic system, Iceland. Nature 517 (7533), 191–195. https://doi.org/10.1038/nature14111. Epub 2014 Dec 15. PMID: 25517098.

Taisne, B., Brenguier, F., Shapiro, N., Ferrazzini, V., 2011. Imaging the dynamics of magma propagation using radiated seismic intensity. Geophys. Res. Lett. 38, L04304. https://doi.org/10.1029/2010GL046068.

Tan, C.T., Taisne, B., Neuberg, J., Basuki, A., 2019. Real-time assessment of potential seismic migration within a monitoring network using Red-flag SARA. J. Volcanol. Geotherm. Res. 384, 31–47. https://doi.org/10.1016/j.jvolgeores.2019.07.004.

Tibaldi, A., 2003. Influence of cone morphology on dikes, Stromboli, Italy. J. Volcanol. Geotherm. Res. 126, 79–95.

Tibaldi, A., 2015. Structure of volcano plumbing systems: a review of multi-parametric effects. J. Volcanol. Geotherm. Res. 298 (2015), 85–135. https://doi.org/10.1016/j.jvolgeores.2015.03.023.

Toledo, T., Jousset, P., Maurer, H., Krawczyk, C., 2020. Optimized experimental network design for earthquake location problems: applications to geothermal and volcanic field seismic networks. J. Volcanol. Geotherm. Res. 391, 106433 https://doi.org/10.1016/j.jvolgeores.2018.08.011.

Tramelli, A., Troise, C., De Natale, G., Orazi, M., 2013. A New Method for Optimization and Testing of Microseismic Networks: an Application to Campi Flegrei (Southern Italy). Bulletin of the Seismological Society of America 103 (3), 1679–1691. https://doi.org/10.1785/0120120211.

Urbani, S., Acocella, V., Rivalta, E., 2018. What drives the lateral versus vertical propagation of dikes? Insights from analogue models. J. Geophys. Res. Solid Earth 123, 3680–3697. https://doi.org/10.1029/2017JB015376.

Valtonen, O., Uski, M., Korja, A., Tiira, T., Kortström, J., 2013. Optimal configuration of a micro-earthquake network. Adv. Geosci. 33, 33–36. https://doi.org/10.5194/adgeo-34-33-2013.

Walsh, B., Jolly, A.D., Procter, J., 2017. Calibrating the amplitude source location (ASL) method by using active seismic sources: an example from Te Maari volcano, Tongariro National Park, New Zealand. Geophys. Res. Lett. 44, 3591–3599. https://doi.org/10.1002/2017GL073000.

Widiwijayanti, C., Win, N.T.Z., Espinosa-Ortega, T., Costa, F., Taisne, B., 2024. The Global Volcano Monitoring Infrastructure Database (GVMID). Frontiers in Earth Science 12, 1284889.

Yamasato, H., 1997. Quantitative analysis of pyroclastic flows using infrasonic and seismic data at Unzen volcano, Japan. J. Phys. Earth 45 (6), 397–416.